Structure and Intermolecular Dynamics of Liquids: Femtosecond Optical Kerr Effect Measurements in Nonpolar Fluorinated Benzenes

Manickam Neelakandan,[†] Debi Pant,[†] and Edward L. Quitevis*[,†,‡]

Department of Chemistry and Biochemistry and Department of Physics, Texas Tech University, Lubbock, Texas 79409

Received: December 11, 1996; In Final Form: February 17, 1997[⊗]

A comparative study of the collective polarizability anisotropy dynamics of benzene, 1,3,5-trifluorobenzene, and hexafluorobenzene was carried out by using optical heterodyne-detected Raman-induced Kerr effect spectroscopy (OHD-RIKES) with 45 fs laser pulses. The OHD-RIKES data were analyzed by using a model-dependent approach and a Fourier transform approach, which yields a spectral density for the liquid. From an analysis of the long-time tails, collective reorientation times of 2.45 ± 0.06, 9.05 ± 0.10, and 13.5 ± 0.1 ps were obtained respectively for C_6H_6, 1,3,5-$C_6F_3H_3$, and C_6F_6. The spectral densities are narrower for 1,3,5-$C_6F_3H_3$ and C_6F_6 than for C_6H_6 by roughly a factor of 2. Information about the intermolecular vibrational modes of the liquid is contained in the reduced spectral density which is obtained by subtracting the tail-matched diffusive reorientational response from the OHD-RIKES data. In the case of C_6H_6 and C_6F_6, the intermolecular spectral density can be decomposed into at least two broad overlapping bands. In contrast, the intermolecular spectral density for 1,3,5-$C_6F_3H_3$ is characterized by a single band. These spectra are rationalized in terms of the librational dynamics of perpendicular dimers in liquid C_6H_6 and C_6F_6 and parallel dimers in liquid 1,3,5-$C_6F_3H_3$.

I. Introduction

The structure and dynamics of aromatic liquids have been the subject of intense investigation for many years. Neutron and X-ray diffraction studies of benzene show that the average molecular arrangement in the liquid is similar to that in the solid.[1,2] In the solid, benzene molecules are oriented perpendicular to each other in an L-shaped geometry. The molecules are arranged in such a way that one hydrogen atom in a molecule is in contact with both a hydrogen atom and a carbon atom in another molecule. Structural models,[1] computer simulations,[3,4] and statistical mechanical calculations[5] of liquid benzene are consistent with molecules being oriented perpendicular to each other in the liquid. Although the structure of a liquid is largely determined by shape-dependent repulsive interactions (i.e., packing effects),[6] the perpendicular arrangement of molecules in liquid benzene can also be rationalized in terms of electrostatic interactions.[7] The dominant multipole interaction between benzene molecules is the electric quadrupole−quadrupole term, which is predicted to be attractive for the T-shaped geometry.[7] Molecular beam electric deflection[8] and Fourier transform microwave[9] measurements support the T-shaped structure for isolated benzene dimers. Ab initio calculations[10] confirm that the T-shaped structure is a stable configuration for the benzene dimer. Recent neutron and X-ray diffraction studies indicate that the quadrupolar interaction is the structure-determining factor in other nonpolar liquid aromatic systems.[2] Such interactions are also important in controlling the stereochemistry of certain organic reactions,[11] binding in model receptors,[12] and the stability of proteins and nucleic acids.[13]

Local order obviously plays a role in determining the intermolecular modes of a liquid. In principle, information about these modes can be gleaned from the high-frequency wings of the depolarized Rayleigh scattering (DRS) spectrum of the liquid. Until recently, this information has been difficult to obtain and to interpret unambiguously, because of the low intensity in the wings of the experimentally measured DRS spectra. Within the past decade, nonlinear optical (NLO) techniques have been developed which use ultrafast lasers that generate sub-50 fs pulses to probe the dynamics of liquids. These techniques include transient grating optical Kerr effect (TG-OKE) spectroscopy,[14] optical-heterodyne-detected Raman-induced Kerr effect spectroscopy (OHD-RIKES),[15−18] position-sensitive Kerr lens spectroscopy,[19] and impulsive stimulated Raman scattering (ISRS).[20−23] Because of the Fourier transform relationship,[17,20c,24,25] time-domain data contain the same information about the dynamics of a liquid as contained in frequency-domain data. NLO techniques have been touted as being superior to DRS, because the short-time dynamics that show up in the wings of the DRS spectrum are greatly enhanced in NLO time-domain data. However, recent advances in light scattering instrumentation have now it possible to obtain the low-frequency intermolecular spectra of liquids from DRS measurements that rival those obtained from OHD-RIKES measurements in terms of quality and signal-to-noise.[25]

TABLE 1: Molecular Parameters for Liquids Studied[a,b]

liquid	I (10^{-46} kg m^2)	Q (10^{-40} C m^2)	α (10^{-40} J V^{-2} m^2)	$\Delta\alpha$ (10^{-40} J V^{-2} m^2)
C_6H_6	14.75	−30	11.56	−6.25
1,3,5-$C_6F_3H_3$	47.5	3.1	11.3	−6.78
C_6F_6	82.1	31.7	11.65	−7.06

[a] References 26, 28, and 29. [b] Symbols: I, moment of inertia; Q, electric quadrupole moment; α, mean polarizability; $\Delta\alpha$, polarizability anisotropy.

Benzene, 1,3,5-trifluorobenzene, and hexafluorobenzene form an insightful triad of molecules in which to probe the effect of local order on the intermolecular dynamics of aromatic liquids. Table 1 lists a few relevant properties for this triad of molecules. These molecules have nearly the same polarizabilities and polarizability anisotropies.[26] As well as being similar in molecular geometry and shape, C_6H_6 and C_6F_6 have similar

* To whom correspondence should be addressed.
[†] Department of Chemistry and Biochemistry.
[‡] Department of Physics.
[⊗] Abstract published in *Advance ACS Abstracts,* April 1, 1997.

S1089-5639(96)04047-9 CCC: $14.00

physical properties.[27] Their electric quadrupole moments are roughly equal in magnitude but opposite in sign.[28,29] These molecules differ in that the moment of inertia of C_6F_6 is ≈5.6 times larger than that of C_6H_6.[29] As we will show below, this partially accounts for the difference between the intermolecular librational dynamics in these two liquids. In contrast, 1,3,5-$C_6F_3H_3$ has a moment of inertia in between that of the other two molecules and has a much smaller electric quadrupole moment.[29] The T-shaped geometry is the favored structure for isolated dimers of C_6F_6,[7] as confirmed by molecular beam electric deflection measurements.[8b] Neutron diffraction data on the liquid are also consistent with C_6F_6 molecules being oriented perpendicular to each other.[2] However, molecular beam electric deflection measurements show that dimers of 1,3,5-$C_6F_3H_3$ are planar with the molecules parallel to each other.[8b] In this configuration, the F atoms are symmetrically staggered, thereby maximizing the stabilization interaction between local C−F dipoles on one molecule with the polarizable C−H and C−C bonds of the other.[7,29a] Although structural measurements for 1,3,5-$C_6F_3H_3$ in either the solid or liquid state are lacking, the parallel or π-stacked geometry is expected to prevail in the liquid. The relative intensities of the far-infrared spectra for these liquids have been recently explained with a model based on these molecular orientations and distributed electric quadrupole moments.[29]

In this article, we present new results from a femtosecond OHD-RIKES study of the collective polarizability anisotropy dynamics of C_6H_6, 1,3,5-$C_6F_3H_3$, and C_6F_6 at room temperature and ambient pressure. The molecular dynamics of liquid C_6H_6 have been extensively studied by using OKE,[15d,l,n,o,18c,22,25,30,32,33] ISRS,[21,22] and stimulated gain spectroscopy (SGS),[31,32] which is a frequency-domain NLO technique. Results from a preliminary OHD-RIKES study of liquid C_6F_6 were reported by us recently.[33] In the present article, we provide a more detailed analysis of the OHD-RIKES response for C_6F_6. This work complements previous NLO investigations[15b,l,n,16d,18c,31] in that the dynamics of nonpolar aromatic liquids as opposed to that of polar aromatic liquids are compared. The article is organized as follows. In section II, a brief description of how the OHD-RIKES data were obtained is given. In section III, the data are presented and discussed. In section IV, the data in the time-domain representation are analyzed using the model-dependent approach. Finally, in section IV, the data in the frequency-domain representation are interpreted in terms of the intermolecular motions associated with plausible models for the local structure in these aromatic liquids.

II. Experimental Methods

Reagent grade C_6H_6, 1,3,5-$C_6F_3H_3$, and C_6F_6 were purchased from Aldrich and used without further purification. The liquids were filtered four times through 0.1 μm syringe filters to remove dust particles. This procedure was essential in reducing the noise in the OHD-RIKES signals due to light scattering from dust particles. The samples were placed in 1 mm path length UV-grade fused silica cells. All measurements were performed at room temperature (≈21 °C) and ambient pressure.

The femtosecond OHD-RIKES measurements were carried out by using linearly polarized ≈45 fs optical pulses centered at ≈800 nm. The pulses were generated via Kerr lens mode locking of a home-built continuous wave Ti:sapphire laser pumped by an all-lines Ar^+ laser.[34] To compensate for group velocity dispersion of the output coupler and the pump−probe optics, the output of the Ti:sapphire laser was directed into a pair of fused silica prisms in a near-retroreflecting geometry. The apparatus used in the OHD-RIKES measurements has been described in an earlier publication[35] and is similar to ones reported previously.[15−18,22,25] The out-of-phase heterodyned signal, which probes the real part of the effective nonlinear susceptibility, was measured. In principle, scans involving oppositely sensed local oscillators must be taken in order to correct for the residual homodyne component.[15m,o] However, we could not detect this residual component with the apparatus in the homodyne configuration (no local oscillator). Therefore, in the analysis of the temporal behavior of the OHD-RIKES data, we assume minimal contamination of the signal by the homodyne component.

The second-order background-free pulse intensity autocorrelation, $G_0^{(2)}(t)$, was measured by replacing the sample with a 100 μm KDP autocorrelation crystal. These scans were used in the analysis of the short-time part of OHD-RIKES data and in the calculation of the spectral densities by the Fourier transform approach.[15h−j,l−q,16b−d,17,18a,c,22,25,35] The pulse autocorrelation was symmetrical and well fitted by a sech^2 function, even after passing through the dispersive optics in the apparatus. The fwhm of the autocorrelation was 70 fs, which corresponds to a pulse width of 45 fs. Such a pulse has a spectral fwhm of ≈230 cm^{-1}.

To determine the femtosecond nondiffusive dynamics, short scans of 1024 points over 3.41 ps were measured, corresponding to 3.33 fs/point. Sixteen scans were averaged to give a final data set. The base line before zero time delay was averaged and subtracted from the data, and the data were then normalized prior to fitting the data. The short scan data were fit to time-dependent model responses. To determine the diffusive dynamics and obtain the low-frequency (0−200 cm^{-1}) spectral densities by the Fourier transform approach, longer scans of 512 points over 9.9 ps corresponding to 19.3 fs/point were taken. For an OHD-RIKES scan covering a total time range of 9.9 ps, fast Fourier transforms (FTT's) can be calculated with a spectral resolution of 1/(9.9 ps) or ≈3.2 cm^{-1}. Because the OHD-RIKES signal and $G_0^{(2)}(t)$ are measured independently, the position of zero time in the data is uncertain.[15m,o,17] In order to handle this uncertainty, the number of data points in the long scans of the OHD-RIKES response and $G_0^{(2)}(t)$ was increased from 512 to 1024 points by performing a cubic spline interpolation of the data prior to the FFT analysis.[15o,17] The position of the $G_0^{(2)}(t)$ peak was shifted relative to that of the coherent spike in the OHD-RIKES signal so as to yield a spectral density that remained positive out to 500 cm^{-1}. In addition, the short scan OHD-RIKES data were extended by grafting long-time tails having the decay behavior of the long scans on to the data. Spectral densities obtained from the FFT of these extended data were used to show the intramolecular depolarized Raman bands. The cubic-spline interpolation, FFT, and nonlinear least-squares fits of long scans were performed by using the plotting/analysis program Horizons.

III. Experimental Results

The transients obtained in NLO time-domain experiments result from the interaction of the femtosecond laser pulse with molecules of the liquid through the third-order nonlinear polarizability $\chi^{(3)}$. In OHD-RIKES, this interaction produces a transient birefringence in the liquid. The birefringence response of the liquid has an instantaneous electronic component (coherent spike) and a noninstantaneous component. The noninstantaneous component is directly related to the time correlation function of the collective polarizability anisotropy which contains information about reorientational and collision-induced dynamics in the liquid.[17,41] The reorientational dynamics can be divided into nondiffusive and diffusive motions. The

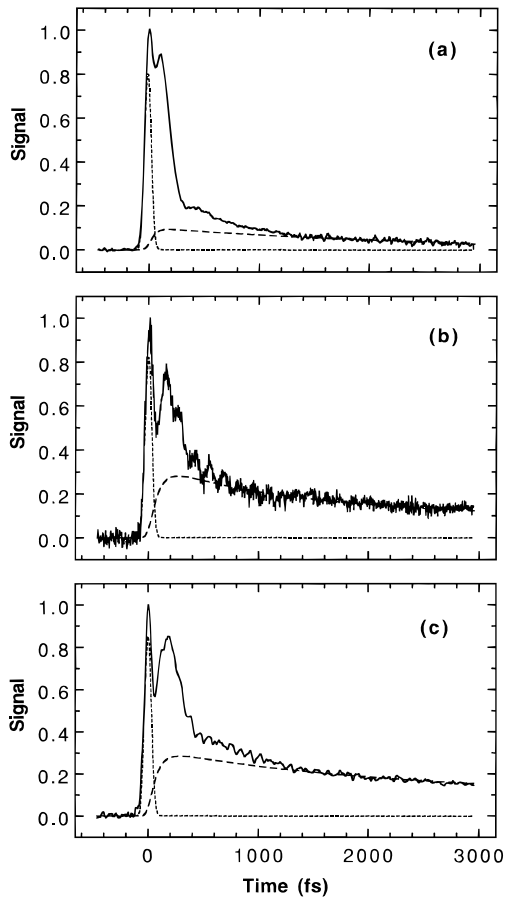

Figure 1. Normalized short scans of OHD-RIKES data at 294 K and ambient pressure for (a) C_6H_6, (b) 1,3,5-$C_6F_3H_3$, and (c) C_6F_6. Data are shown with the second-order background free pulse intensity autocorrelation (short-dashed curve) and the diffusive response (long-dashed curve).

nondiffusive reorientational dynamics include inertially limited rotations and librations which can be overdamped or underdamped. All of these motions contribute to the short-time response (<1 ps) of the birefringence signal, whereas the long-time decay (>1 ps) of the birefringence signal is primarily determined by the diffusive reorientational dynamics.

Short scans of the OHD-RIKES responses for liquid C_6H_6, 1,3,5-$C_6F_3H_3$, and C_6F_6 are plotted in Figure 1, along with the pulse autocorrelation (short-dashed curve). The tail-matched diffusive responses (long-dashed curves) are also shown with the data. The response for C_6H_6 compares well with OHD-RIKES data obtained previously by other researchers.[15d,l,18c,22,25] The intensities of the pulse autocorrelation and the diffusive response relative to that of the OHD-RIKES signal were determined by fitting the OHD-RIKES signal to the sum of electronic and nuclear responses as described below. The instantaneous response is due to the electronic hyperpolarizability. The rising edge of the autocorrelation trace closely matches the rising edge of the OHD-RIKES signal. Superimposed on the electronic response is the noninstantaneous nuclear response. The peak of the nuclear response is associated with the intermolecular librational dynamics of the liquid. This peak occurs at ≈110 fs in C_6H_6, ≈160 fs in 1,3,5-$C_6F_3H_3$, and ≈190 fs in C_6F_6.

Within 100 fs, the signal for C_6H_6 rapidly decays from the librational peak to 20% of the maximum signal amplitude and evolves into an intermediate response with an average decay time of 500 fs. The intermediate response then gives way to the diffusive response. A weak secondary oscillation at ≈400 fs is superimposed on this intermediate response. This weak oscillation can be attributed to an intermolecular librational mode.[21,32] The behavior of this OHD-RIKES data is consistent with results from previous NLO studies of liquid C_6H_6.[15d,l,18c,22,25] In contrast, the signals for 1,3,5-$C_6F_3H_3$ and C_6F_6 decay from the librational peak to 35−40% of the maximum signal amplitude, taking roughly twice as long to do so. The slow oscillation due to the intermolecular librational mode which is seen in the OHD-RIKES data for C_6H_6 is noticeably absent in the OHD-RIKES data for these other two liquids.

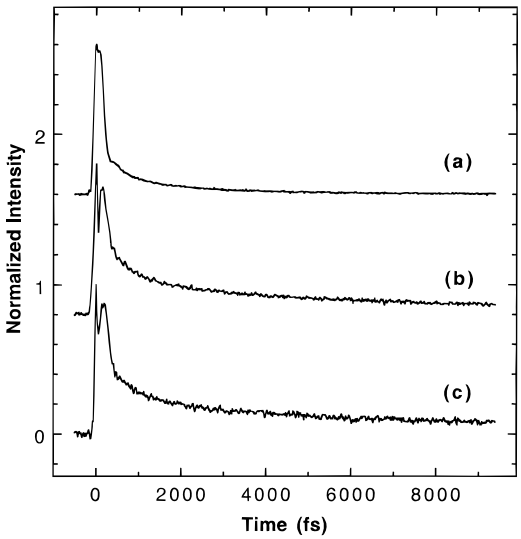

Figure 2. Normalized and offset long scans of OHD-RIKES data for (a) C_6H_6, (b) 1,3,5-$C_6F_3H_3$, and (c) C_6F_6.

TABLE 2: OHD-RIKES Long-Time Parameters[a,b]

liquid	N	f_1	τ_1 (ps)	f_2	τ_2 (ps)	χ^2
C_6H_6	0.107	1.0	2.45			0.004
1,3,5-$C_6F_3H_3$	0.417	0.542	1.05	0.458	9.05	0.020
C_6F_6	0.319	0.514	1.73	0.486	13.5	0.056

[a] See eq 1 for definition of fit parameters. [b] Fits were obtained for $t \geq 2$ ps.

Long scans of the OHD-RIKES response for C_6H_6, 1,3,5-$C_6F_3H_3$, and C_6F_6 are shown in Figure 2. To determine the diffusive dynamics in these liquids, least-squares fits of the long-time tails ($t > 2$ ps) to a multiexponential decay function

$$R(t) = N\sum_i f_i \exp(-t/\tau_i) \qquad (1)$$

were carried out, where N is a constant which accounts for the relative intensities of the OHD-RIKES signals and the f_i's give the fractional contribution of each exponential term. Fit parameters are given in Table 2, with typical fits shown in Figure 3. The long-time tail of the OHD-RIKES signal for C_6H_6 is well fit by a single-exponential decay function with a 1/e time constant of 2.45 ± 0.06 ps. The value of this time constant agrees with the value of 2.4 ps obtained in previous OHD-RIKES measurements[15d,l] and is consistent with the collective reorientation time of 3.0 ps obtained from DRS measurements.[36−39] A best fit of the long-time tails of the OHD-RIKES signals for 1,3,5-$C_6F_3H_3$ and C_6F_6 was obtained by using biexponential decay functions with short and long components. The slow component can be assigned to the collective reorientation time in the liquid. The 13.5 ± 0.1 ps component in the OHD-RIKES data for C_6F_6 compares well with the value of 14.0 ps obtained previously from DRS measurements.[36,37] From the OHD-RIKES data, a reorientation time of 9.05 ± 0.10 ps is obtained for liquid 1,3,5-$C_6F_3H_3$. In contrast to the other

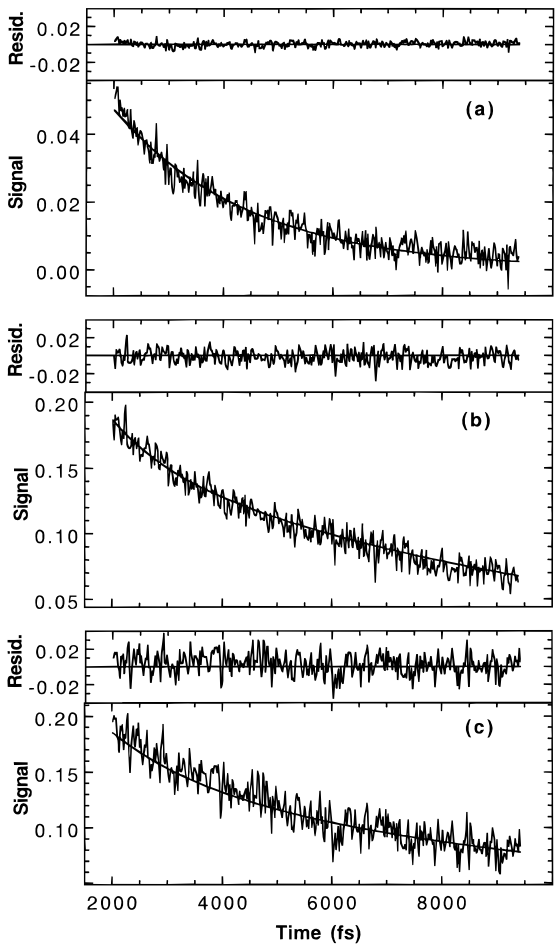

Figure 3. Typical fits of the diffusive part of the OHD-RIKES data for (a) C_6H_6, (b) 1,3,5-$C_6F_3H_3$, and (c) C_6F_6. The residuals for the fits are plotted above the corresponding data. See Table 2 for fit parameters.

two liquids, there are very few reported time-domain measurements of the reorientational dynamics in liquid 1,3,5-$C_6F_3H_3$. Raman spectral bandwidth data for the two a′ vibrations of 1,3,5-$C_6F_3H_3$ yield a reorientation time of 6.7 ps at 296 K.[40] The reorientation time is extracted in the usually way by subtracting the line width of the isotropic Raman band from that of the depolarized Raman band. Although this value of the reorientation time is less than the value obtained in this study, it is not unreasonable, given that reorientation times from Raman line shapes are not as accurate as those obtained directly from the diffusive part of OHD-RIKES response.

For symmetric top molecules, the diffusive reorientational component of the OHD-RIKES response should be characterized by a single reorientation time for motion about an axis normal to the symmetry axis of the molecule. If the slow component of the long-time OHD-RIKES response for these two liquids is ascribed to diffusive reorientation, the 1.43 and 1.73 ps decay constants in the long-time OHD-RIKES response for 1,3,5-$C_6F_3H_3$ and C_6F_6 must be due to the slow relaxation of some other intermolecular mode. One possibility is that the amplitude of the 1−2 ps relaxation process arises from translational interaction-induced (I-I) effects which decay on the time scale of local density fluctuations in the liquid.[15c−e] Molecular dynamics simulations on liquid CH_3CN show that the I−I contributions to the polarizability anisotropy correlation function decay slowly and contribute to the signal at long times.[41]

In the OHD-RIKES data for 1,3,5-$C_6F_3H_3$ and C_6F_6, faster oscillations are superimposed on the contribution from the intermolecular motion. These oscillations arise from the coherent excitation of intramolecular vibrational Raman modes.[15c,i,o,17,18,22] Specifically, Raman modes with fundamental frequencies that lie within the spectral width of the laser pulse are excited. The Raman mode that is excited in 1,3,5-$C_6F_3H_3$ is the depolarized e″ intramolecular ring deformation at 253.4 cm^{-1}.[42] The Raman mode that is excited in C_6F_6 is the depolarized e_{1g} C−F out-of-plane bending motion at 370 cm^{-1}.[43] In the case of C_6H_6, the lowest frequency Raman mode with the strongest intensity is the depolarized e_{2g} C−C in-plane bending motion at 606 cm^{-1}.[44] The absence of this Raman-active intramolecular vibrational mode in the C_6H_6 OHD-RIKES data is due to the fact that the mode does not lie within the bandwidth of the laser pulses used in this study. Oscillations corresponding to this bending mode in C_6H_6 have however been observed for excitation with 20 fs pulses.[22]

IV. Analysis and Discussion

A. Temporal Response. To provide a more quantitative description of the short-time dynamics, the finite pulse width of the laser must be taken into account. For pump, probe, and local oscillator pulses derived from a single transform-limited optical pulse, the OHD-RIKES signal is the convolution of $G_0^{(2)}(t)$ and the molecular nonlinear response $R(t)$:

$$T(\tau) \propto \int_{-\infty}^{\infty} G_0^{(2)}(t)\, R(\tau - t)\, \mathrm{d}t \tag{2}$$

For optical pulses far from an electronic resonance, the impulse response $R(t)$ can be written as the sum of an electronic response function $\sigma(t)$ and a nuclear response function $r(t)$:

$$R(t) = \sigma(t) + r(t) \tag{3}$$

If the electronic response function is instantaneous on the time scale of the laser pulse, the electronic response function can be represented by a δ-function:

$$\sigma(t) = A_0 \delta(t) \tag{4}$$

where A_0 is proportional to the electronic hyperpolarizability. The total noninstantaneous nuclear response for these liquids can be empirically modeled by a superposition of terms:

$$r(t) = \sum_i A_i r_i(t) \tag{5}$$

This model-dependent approach has been used previously to describe the OHD-RIKES responses of many liquids composed of anisotropic molecules.[15c−f,16a,b] The $r_i(t)$ in eq 5 are given by

$$r_1(t) = \sum_i f_i \exp(-t/\tau_i^{\mathrm{diff}})[1 - \exp(-2t/\beta_1)] \tag{6}$$

$$r_2(t) = \exp(-t/\tau_{\mathrm{int}})[1 - \exp(-2t/\beta_2)] \tag{7}$$

$$r_3(t) = \exp(-t/\tau_{\mathrm{lib}}) \exp(-\Delta^2 t^2/2) \sin(\omega_0 t) \tag{8}$$

The functions $r_1(t)$ and $r_2(t)$ are assigned to the diffusive and intermediate responses observed in the OHD-RIKES signals. For anisotropic molecules, the intermediate response has been attributed to the constructive interference of critically damped and overdamped collective intermolecular vibrational modes.[15j,k] The parameters $\beta_1/2$ and $\beta_2/2$ are the rise times for the diffusive and intermediate responses and account for the fact that the nuclear responses cannot follow the intensity profile of these short laser pulses.[15d,e,j,l,16a,b]

I−I effects can also contribute to the intensity of this intermediate response[15c−f,16a,b] These effects arise from distortions of the molecular polarizabilities due to the interactions of neighboring molecules and will depend in general on the translational and orientational degrees of freedom. In atomic liquids, the amplitude of the OKE response clearly arises from translational I−I effects.[45] As mentioned above, the signal contribution due to translational I−I effects will exhibit a relaxation time characteristic of local density fluctuations. It is very difficult to determine the extent to which I−I effects contribute to the intermediate response in liquids. However, the intensity due the intermolecular librational modes should be larger than the I−I intensity in the nondiffusive part of the OHD-RIKES signal for liquids composed of anisotropic molecules.[15o] Attempts have been made to assess the contribution of translational I−I modes to experimental OHD-RIKES data by comparison to molecular dynamics simulations.[46]

The oscillatory response function $r_3(t)$ represents a coherently driven, Raman-active, intermolecular librational motion.[15d−f] It is based on a simple model involving the "cage"-induced reversal of angular momentum.[47] The function is an approximation to the coherent librational amplitude which is given by the superposition of damped/dephased oscillators (homogeneous broadening) in a distribution of molecular environments (inhomogeneous broadening). In this response function, ω_0 is the mean librational frequency and τ_{lib} is an average dephasing time for the oscillators and contains contributions from pure dephasing due to fluctuations in cage structures and population relaxation. The Gaussian function reflects the distribution of molecular cages in a disordered liquid that gives rise to different librational frequencies. The parameter Δ in this function is the inhomogeneous dephasing rate, which is a measure of the distribution of oscillator frequencies. The fwhm of the inhomogeneous distribution $\Delta\tilde{\nu}$ is related to Δ by

$$\Delta\tilde{\nu} = \Delta(2 \ln 2)^{1/2}/\pi c \tag{9}$$

Using eqs 2−8, the data were analyzed as follows. Rise times can be estimated from either the free rotation time of the molecule or from the ensemble-averaged intermolecular vibrational frequency. In this study, β_1 and β_2 were set equal to $1/\langle\Delta\omega\rangle$, where $\langle\Delta\omega\rangle$ is the first moment of the low-frequency spectral density.[16a,b] The pulse autocorrelation was convoluted with the diffusive response function $r_1(t)$ using the fit parameters in Table 2. This diffusive component was then tail-matched to the OHD-RIKES signal. The long dashed curves in Figure 1 are the tail-matched diffusive components. A reduced data set was then generated by subtracting the tail-matched long component from the OHD-RIKES signal.[15c,k,l] From a semilogarithmic plot of the reduced data set, the 1/e time constant for the intermediate response was obtained. Next, the pulse autocorrelation was convoluted with the response function $r_2(t)$, with τ_{int} set equal to the 1/e time constant obtained from the semilogarithmic plot of the reduced data set. This intermediate component was tail-matched to the reduced set. Finally, a best fit of the convolution of the pulse autocorrelation and the total response function

$$R(t) = A_0\delta(t) + A_1 r_1(t) + A_2 r_2(t) + A_3 r_3(t) \tag{10}$$

was obtained by varying the coefficients A_0 and A_3 and the constants τ_{lib}, Δ, and ω_0, with the other constants held fixed. This procedure yielded good fits of the OHD-RIKES signals for 1,3,5-$C_6F_3H_3$ and C_6F_6, as shown in Figure 4. Unfortunately, we were unable to obtain good agreement with the C_6H_6 data by using just three model response functions. The OHD-RIKES

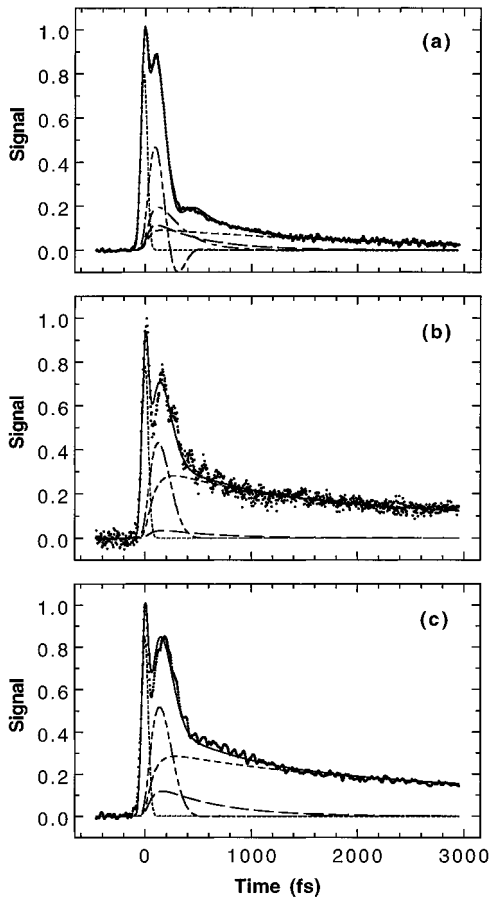

Figure 4. Fit (solid line) of OHD-RIKES data (points) together with the corresponding component responses $\sigma(t)$ and $r_1(t)-r_3(t)$ (dashed lines) for (a) C_6H_6, (b) 1,3,5-$C_6F_3H_3$, and (c) C_6F_6. See Tables 3 and 4 for fit parameters.

response of C_6H_6 is clearly more complicated than that of 1,3,5-$C_6F_3H_3$ or C_6F_6. A better fit of the C_6H_6 data was obtained when a function of the form

$$r_3(t) = \exp(-\Delta^2 t^2/2)\sin(\omega_0 t) \tag{11}$$

was used to model the librational response, with another intermediate response term added to the total nuclear response function in eq 5. Equation 11 describes a situation in which the dephasing processes are slower than the librational dynamics, and because of inhomogeneities in the local environments, there is a distribution of oscillators. In this case, the librational dynamics is dominated by inhomogeneous dephasing.[48] Such a four-term model has been used previously to fit ISRS data for several liquids, including C_6H_6.[20a,b,d,21] As can be seen in Figure 4, the fit, although not exact, reproduces the main features of the data reasonably well. The fit parameters for the short-time OHD-RIKES data are summarized in Tables 3 and 4. For C_6H_6, 1,3,5-$C_6F_3H_3$, and C_6F_6 the librational frequencies are respectively, 69, 31, and 33 cm^{-1}.

In our analysis of the librational response for C_6H_6, a fit of the data was obtained by setting $\Delta\tilde{\nu} \approx 48$ cm^{-1}. This corresponds to an inhomogeneous dephasing rate of 3.9 ps^{-1}. In the case of 1,3,5-$C_6F_3H_3$ and C_6F_6, the parameter $\Delta\tilde{\nu}$ was arbitrarily set equal to 48 cm^{-1}, and the dephasing time τ_{lib} varied to fit the librational response for these two liquids. This approach leads to the dephasing time being longer in C_6F_6 than in 1,3,5-$C_6F_3H_3$ (600 vs 400 fs). This result is physically reasonable, if one interprets τ_{lib} to be on the order of the fluctuation time for cage structures in the liquid. Because C_6F_6

TABLE 3: OHD-RIKES Parameters for Electronic and Diffusive Responses[a]

liquid	electronic response A_0	diffusive response[b] A_1	f_1	τ_1^{diff} (ps)	f_2	τ_2^{diff} (ps)	β_1 (fs)
C_6H_6	0.9758 ± 0.0188	0.0016 ± 0.0001	1.00	2.45 ± 0.06			96 ± 20
1,3,5-$C_6F_3H_3$	0.9763 ± 0.0391	0.0054 ± 0.0003	0.54 ± 0.10	1.05 ± 0.10	0.46 ± 0.01	9.05 ± 0.30	165 ± 20
C_6F_6	0.9750 ± 0.0172	0.0047 ± 0.0001	0.51 ± 0.10	1.73 ± 0.05	0.49 ± 0.06	13.5 ± 0.1	188 ± 15

[a] See eqs 4−6 for definition of parameters. [b] Diffusive parameters obtained from fit of long-time response (see Table 2).

TABLE 4: OHD-RIKES Parameters for Intermediate and Librational Responses[a,b]

	intermediate response			librational response					
liquid	A_{2a} / A_{2b}	τ_{int}^a (fs) / τ_{int}^b (fs)	β_2^a (fs) / β_2^b (fs)	A_3	$\tilde{\nu}_0$[c] (cm^{-1})	τ_{lib} (fs)	γ[d] (ps^{-1})	Δ (ps^{-1})	$\Delta\tilde{\nu}$[e] (cm^{-1})
C_6H_6	0.0025 ± 0.0002	468 ± 30	96 ± 8	0.0098 ± 0.0002	69 ± 5			3.9 ± 0.3	48 ± 4
	0.0103 ± 0.0006	200 ± 20	300 ± 20						
1,3,5-$C_6F_3H_3$	0.0009 ± 0.0004	500 ± 100	165 ± 20	0.0174 ± 0.0017	31 ± 5	400 ± 50	2.5 ± 0.3	3.9 ± 0.3	48 ± 4
C_6F_6	0.0028 ± 0.0003	558 ± 45	147 ± 20	0.0175 ± 0.0002	33 ± 3	600 ± 50	1.7 ± 0.1	3.9 ± 0.3	48 ± 3

[a] See eqs 7−11 for definition of parameters. [b] $A_0 + A_1 + A_{2a} + A_{2b} + A_3 = 1$. [c] $\tilde{\nu}_0 = \omega_0/2\pi c$. [d] $\gamma = 1/\tau_{lib}$. [e] $\Delta\tilde{\nu} = \Delta(2 \ln 2)^{1/2}/(\pi c)$.

molecules are more massive than 1,3,5-$C_6F_3H_3$ molecules, they will move more slowly in the liquid at a given temperature. Therefore, cage structures should fluctuate more slowly in liquid C_6F_6 than in liquid 1,3,5-$C_6F_3H_3$. In contrast to C_6H_6, the intermolecular librational dynamics in C_6F_6 and 1,3,5-$C_6F_3H_3$ are not strongly dominated by inhomogeneous dephasing. The value of the homogeneous dephasing rate γ, which is given by $1/\tau_{lib}$, is $\approx$2.5 ps^{-1} in 1,3,5-$C_6F_3H_3$ and $\approx$1.7 ps^{-1} in C_6F_6. These values are comparable in magnitude to the value of the inhomogeneous dephasing rate of 3.9 ps^{-1} in these liquids.

As can be seen from Table 4, all three liquids exhibit an intermediate response, $r_{2a}(t)$, having roughly the same 1/e time constant ($\tau_{int}^a \approx 0.5$ ps). This suggests that the intermolecular motion giving rise to this response must be the same for all three liquids. In contrast, the parameters that characterize the second term in the intermediate response for C_6H_6 (A_{2b}, β_2^b, and τ_{int}^b) are very different than the parameters that characterize the first term. This second intermediate term, $r_{2b}(t)$, must be due to an intermolecular motion which is not present in the other two liquids. It is evident from Figure 4 that the intermediate response is more important in determining the nondiffusive dynamics in C_6H_6 and C_6F_6 than in 1,3,5-$C_6F_3H_3$. Based on the amplitudes, the intermediate response contributes to 53% of the nuclear response in C_6H_6 and to 11% of the nuclear response in C_6F_6, whereas it contributes to only 3% of the nuclear response in 1,3,5-$C_6F_3H_3$.

To further understand the librational dynamics in these liquids, we will assume the librational frequency is simply given by $(k/I)^{1/2}$, where I is the moment of inertia of the molecule for motion perpendicular to the symmetry axis and k is the force constant which characterizes the intermolecular potential governing the librational motion of the molecule in the liquid. Obviously, in a liquid, the actual potential will be extremely complicated because of many-body interactions. Let us first compare the librational dynamics in C_6H_6 and C_6F_6. The ratio of force constants for this pair is given by

$$\frac{k(C_6F_6)}{k(C_6H_6)} = \left[\frac{\omega_0(C_6F_6)}{\omega_0(C_6H_6)}\right]^2 \frac{I(C_6F_6)}{I(C_6H_6)} \tag{12}$$

Using the values of the moment of inertia given in Table 1 and the librational frequencies given in Table 4, one gets that the value for the force constant ratio in eq 12 is equal to $\approx$0.8. This value is reasonable, given the similarity of the structures of these two liquids. The properties of the potential will be determined by both repulsive and attractive interactions. We will assume however that the attractive interactions largely determine the dynamics in aromatic liquids. For nonpolar aromatic liquids, the electric quadrupole−quadrupole interaction term should be the dominant term in the intermolecular potential. This should be especially true for C_6H_6 and C_6F_6 because of their large quadrupole moments (Table 1). The electrostatic interactions in C_6H_6 and C_6F_6 are rather unique in that their quadrupole moments are of the same magnitude but opposite in sign. Thus, it is not surprising that the force constant for the librational motion in C_6H_6 is roughly comparable to that in C_6F_6.

Since the molecules in liquid 1,3,5-$C_6F_3H_3$ tend to form parallel structures instead of L-shaped structures, the intermolecular potential that governs the librational motion in liquid 1,3,5-$C_6F_3H_3$ should be different than that in liquid C_6H_6 or liquid C_6F_6. This difference should be evident in the force constant ratios between 1,3,5-$C_6F_3H_3$ and C_6H_6 and between 1,3,5-$C_6F_3H_3$ and C_6F_6:

$$\frac{k(C_6F_3H_3)}{k(C_6H_6)} = \left[\frac{\omega_0(C_6F_3H_3)}{\omega_0(C_6H_6)}\right]^2 \frac{I(C_6F_3H_3)}{I(C_6H_6)} \tag{13}$$

$$\frac{k(C_6F_3H_3)}{k(C_6F_6)} = \left[\frac{\omega_0(C_6F_3H_3)}{\omega_0(C_6H_6)}\right]^2 \frac{I(C_6F_3H_3)}{I(C_6F_6)} \tag{14}$$

Using the values of the moment of inertia listed in Table 1 and librational frequencies listed in Table 4, one gets values of $\approx$0.65 and $\approx$1.6 for the force constant ratios in eqs 13 and 14, respectively. Therefore, the potential that governs the librational motion is flatter at the minimum in liquid 1,3,5-$C_6F_3H_3$ than in liquid C_6H_6, whereas it is sharper at the minimum in liquid 1,3,5-$C_6F_3H_3$ than in liquid C_6F_6. These relative differences in the force constants are surprisingly small, if one considers the fact that the quadrupole moment of 1,3,5-$C_6F_3H_3$ is $\approx$10 times smaller in magnitude than the quadrupole moment of either C_6H_6 or C_6F_6. The small relative difference in the force constants can be rationalized in terms of the tendency of 1,3,5-$C_6F_3H_3$ molecules to stack parallel to each other. Because this geometry places the C−F bond dipoles on one molecule in close proximity to the C−H bond dipoles on the other molecule, the molecules will be attracted to each other more strongly, thereby giving rise to a much larger force constant than one would predict on the basis of point quadrupole interactions.

B. Spectral Response. A multiparameter curve fitting approach to the analysis of the time-domain data suffers from the problem that different parameters can compensate for each

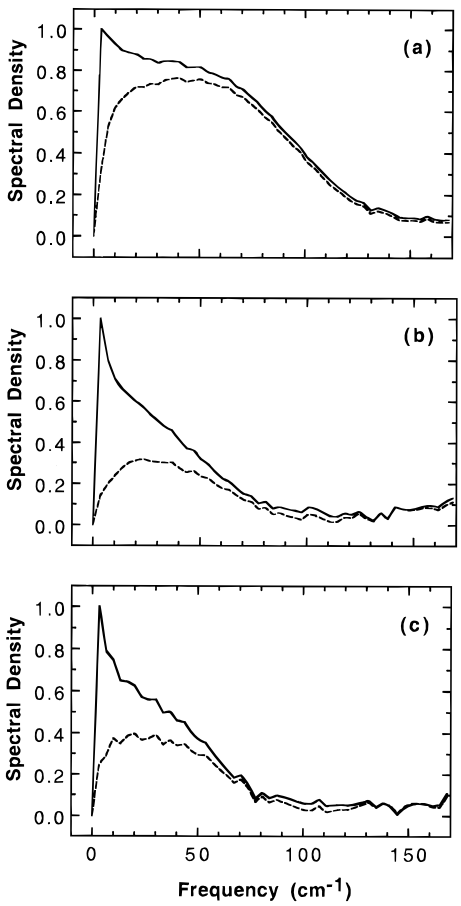

Figure 5. Spectral densities obtained from OHD-RIKES data by using the Fourier transform technique: (a) C_6H_6, (b) 1,3,5-$C_6F_3H_3$, and (c) C_6F_6. Solid curves are the full spectral densities, and dashed curves are the reduced spectral densities. See Table 5 for summary of spectral parameters (first moment and fwhm).

other, making it difficult to arrive at a unique interpretation of the data.[15l] An alternate procedure to analyzing the OHD-RIKES data that avoids this problem is the Fourier transform technique.[15h−j,l−q,16b−d,17,18a,c,22,25,35] The result of this approach is a spectral density. The Fourier transform of eq 2 gives the product

$$F\{T(\tau)\} = F\{G_0^{(2)}(t)\}\ F\{R(t)\} \qquad (15)$$

where F denotes a forward complex Fourier transform operation. The deconvolution is accomplished by computing the complex quotient

$$F\{T(\tau)\}/F\{G_0^{(2)}(t)\} = F\{R(t)\} \equiv D(\Delta\omega) \qquad (16)$$

where $\Delta\omega$ is the frequency relative to the laser center frequency. $D(\Delta\omega)$ represents the intrinsic frequency response to a spectrally flat, δ-function excitation pulse. If one assumes that the impulse response can be written as the sum of an electronic response and a nuclear response (eq 3), $D(\Delta\omega)$ can be expressed as the sum of a constant A_0 and the Fourier transform of the nuclear response function,

$$D(\Delta\omega) = A_0 + F\{r(t)\} \qquad (17)$$

Since A_0 is real, the electronic hyperpolarizability will not contribute to Im$[D(\Delta\omega)]$. Information about all possible nuclear motions is contained in the spectral density Im$[D(\Delta\omega)]$.

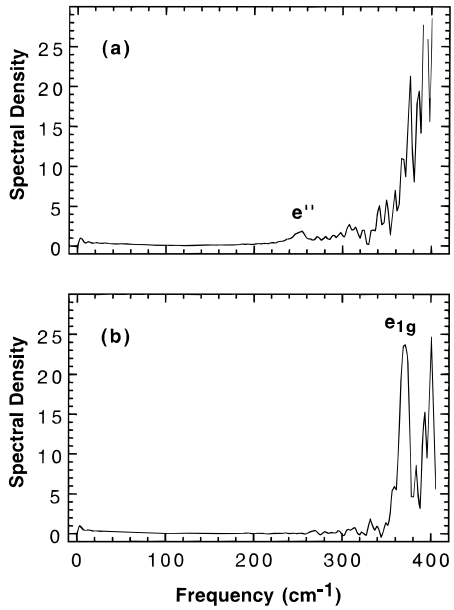

Figure 6. Expanded plot of the full spectral densities for (a) 1,3,5-$C_6F_3H_3$ showing an intramolecular band at ≈253 cm^{-1} which is assigned to the depolarized e″ ring deformation mode and for (b) C_6F_6 showing an intramolecular band at ≈370 cm^{-1} which is assigned to the e_{1g} C−F out-of-plane bending motion.

TABLE 5: Comparison of Spectral Density Parameters[a,b]

liquid	first spectral moment (cm^{-1})	fwhm[c] (cm^{-1})
C_6H_6	55/59	91/81
1,3,5-$C_6F_3H_3$	32/40	50/56
C_6F_6	36/41	46/63

[a] The first number in each entry is the value corresponding to the full spectral density Im$[D(\Delta\omega)]$. The second number is the value for the reduced spectral density Im$[D'(\Delta\omega)]$. [b] Error = ±1 cm^{-1}. [c] Full width at half-maximum.

Figure 5 illustrates the low-frequency part of Im$[D(\Delta\omega)]$ between 0 and 150 cm^{-1} (solid curves) obtained from the FFT of the OHD-RIKES data. The spectral densities are sharply peaked near the origin. This feature is the pure diffusive reorientational response. Figure 6 illustrates the spectral response for liquid 1,3,5-$C_6F_3H_3$ and C_6F_6 over the extended frequency range 0−400 cm^{-1}. Despite the large-amplitude structure that arises from the noise in the short scan OHD-RIKES data, the intramolecular vibrational bands are readily apparent. The peak that occurs at ≈253 ± 1 cm^{-1} in the 1,3,5-$C_6F_3H_3$ spectral density is assigned to the depolarized e″ intramolecular ring deformation mode.[42] Similarly, the peak at ≈370 ± 1 cm^{-1} in the spectral density for C_6F_6 is assigned to the depolarized e_{1g} C−F out-of-plane motion in the molecule.[43] As discussed above, these modes appear as oscillations in the OHD-RIKES signals for these liquids (see Figure 1b,c).

Values of the first spectral moment $\langle\Delta\omega\rangle$ were calculated for these liquids from the data illustrated in Figure 5. These are listed in Table 5 along with values of the fwhm for the spectral density. The values of $\langle\Delta\omega\rangle$ were used to estimate the rise times β_i in eqs 6 and 7. To isolate the contribution of the intermolecular vibrational dynamics of these liquids, it is useful to apply the Fourier transform technique to the reduced OHD-RIKES data (data minus diffusive component) to obtain the reduced spectral density, Im $[D'(\Delta\omega)]$ (dashed curves in Figure 5). The reduced spectral density gives the pure Raman-active vibrational modes of the liquid.[15h−q] Table 5 lists values of the fwhm and the first moment of the reduced spectral density. The spectral densities for aromatic liquids tend to be wider than that of

TABLE 6: Line Shape Parameters for Fit of Reduced Spectral Densities[a,b]

liquid	A_{BL}	a	ω_1 (cm^{-1})	A_G	ω_2 (cm^{-1})	ϵ (cm^{-1})
C_6H_6	0.124 ± 0.006	1.06 ± 0.02	9.7 ± 0.2	1.34 ± 0.02	33.0 ± 0.5	49.0 ± 0.5
1,3,5-$C_6F_3H_3$	0.099 ± 0.001	1.07 ± 0.01	22.5 ± 0.5			
C_6F_6	0.33 ± 0.02	0.59 ± 0.02	27 ± 2	0.29 ± 0.04	47 ± 3	16 ± 2

[a] See eqs 19 and 20 for definition of fit parameters. [b] Fits were obtained for $0 \le \Delta\omega \le 160$ cm^{-1} (C_6H_6), $0 \le \Delta\omega \le 100$ cm^{-1} (1,3,5-$C_6F_3H_3$), and $0 \le \Delta\omega \le 125$ cm^{-1} (C_6F_6). Outside of these ranges, the spectral densities do not approach the base line in a physically reasonable way. This can be attributed to a mismatch in the optics in the pump and probe lines of the interferometer. This artifact, however, does not affect our analysis or interpretation of the intermolecular vibrational bands.

nonaromatic liquids.[18c,32] Cong et al.,[18c] in a comparative OHD-RIKES study of benzene and polar benzene derivatives, attributed the broadness of the spectral density to the highly anisotropic nature of the intermolecular potential in these liquids which arises from the polarizability of the π-electrons in the benzene ring. However, our results show that the spectral densities for these nonpolar fluorinated benzene derivatives are roughly half as wide as the spectral density for C_6H_6. As noted above, the polarizability and polarizability anisotropies are nearly the same for these liquids. Other factors must therefore play a role in determining the broadening mechanism in these liquids, besides the polarizability of the π-electrons.

Removing the low-frequency diffusive component results in the width and first spectral moment of the reduced spectral density being greater than that of the full spectral density (Table 5). For 1,3,5-$C_6F_3H_3$ and C_6F_6 the values of first spectral moment obtained from the reduced spectral density are in good agreement with the values of the mean librational frequency obtained in the model-dependent analysis of the OHD-RIKES. The difference between the full spectral density and reduced spectral density for each liquid can be rationalized in terms of the relative contributions of the various response components to the time-domain data. For example, based on the amplitudes, the contribution of the diffusive component to the overall nuclear response is 17−19% for 1,3,5-$C_6F_3H_3$ and C_6F_6, but only 7% for C_6H_6. Consequently, the difference between the mean frequencies and widths of Im[$D(\Delta\omega)$] and Im[$D'(\Delta\omega)$] for C_6H_6 are not as pronounced as they are for 1,3,5-$C_6F_3H_3$ and C_6F_6.

To provide a more quantitative description of the intermolecular bands in the Im[$D'(\Delta\omega)$] spectra, nonlinear least-squares fits of the band profiles to various line shapes were carried out. The best fits obtained from this analysis are shown in Figure 7 with the fit parameters given in Table 6. We find that the intermolecular vibrational band in both liquid C_6H_6 and C_6F_6 is well described by the sum of two bands:

$$\mathrm{Im}[D'(\Delta\omega)] = I_{BL}(\Delta\omega) + I_G(\Delta\omega) \qquad (18)$$

where $I_{BL}(\Delta\omega)$ is the line shape function,

$$I_{BL}(\Delta\omega) = A_{BL}(\Delta\omega)^a \exp(-\Delta\omega/\omega_1) \qquad (19)$$

and $I_G(\Delta\omega)$ is the antisymmetrized Gaussian line shape function,

$$I_G(\Delta\omega) = A_G\{\exp[-(\Delta\omega - \omega_2)^2/2\epsilon^2] - \exp[-(\Delta\omega + \omega_2)^2/2\epsilon^2]\} \qquad (20)$$

Both functions go to zero at zero frequency as required by Im[$D'(\Delta\omega)$]. This spectral decomposition of the reduced spectral density for C_6H_6 is consistent with previous OHD-RIKES data of McMorrow and Lotshaw.[15l,n] Other line shape functions were tried, but these did not fit the data as well as those in eqs 19 and 20. The line shape functions in eqs 19 and 20 have been used previously to describe the OHD-RIKES[16d] and SGS[31] spectra of other liquids. The line shape function

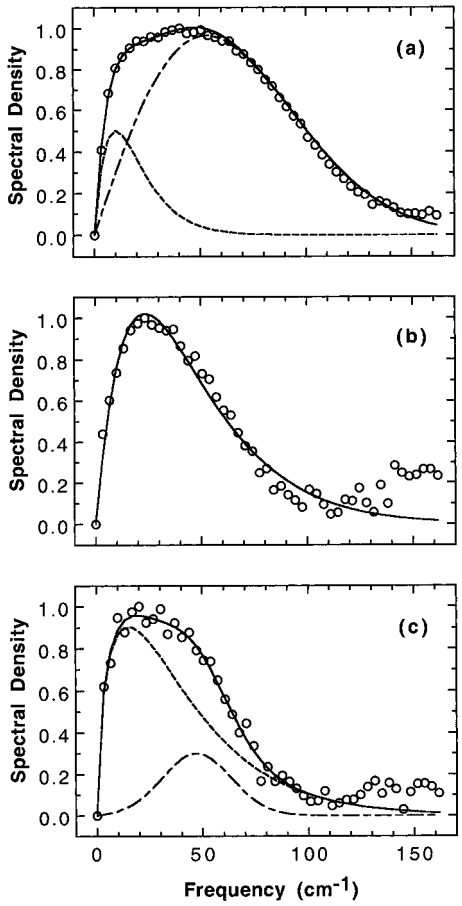

Figure 7. Fits of the reduced spectral densities for (a) C_6H_6 to two bands, (b) 1,3,5-$C_6F_3H_3$ to a single band, and (c) C_6F_6 to two bands. See Table 6 for fit parameters.

$I_{BL}(\Delta\omega)$ was originally introduced by Bucaro and Litovitz[49] to account for collision-induced contributions to DLS spectra in liquids. However, in this analysis, $I_{BL}(\Delta\omega)$ is just treated as an empirical fitting function.

The data suggest that the intermolecular vibrational spectrum for these two liquids arises from at least two vibrational modes. Because C_6H_6 and C_6F_6 are similar in structure, these intermolecular modes must be also the same in these two liquids. In liquid C_6H_6, the high-frequency component, which peaks at ≈54 cm^{-1} and has a fwhm of ≈85 cm^{-1}, dominates the low-frequency component, which peaks at ≈10 cm^{-1} and has a fwhm of 24 cm^{-1}. Comparing areas under the component bands, the 54 cm^{-1} component is 5.6 times larger than the 10 cm^{-1} component and contributes to 85% of the total area of the intermolecular band in C_6H_6. In liquid C_6F_6, the situation is reversed with the low-frequency component, which peaks at ≈16 cm^{-1} and has a fwhm of 52 cm^{-1}, dominating the high-frequency component, which peaks at ≈47 cm^{-1} and has a fwhm of 28 cm^{-1}. Comparing areas under the component bands, the 16 cm^{-1} component is 4.6 times larger than the 47 cm^{-1} and

contributes to 82% of the total area of the intermolecular band in C_6F_6.

In the case of 1,3,5-$C_6F_3H_3$, the intermolecular vibrational band at $\approx$47 cm^{-1} in the reduced spectral density does not rise sharply on the low-frequency side as it does for C_6H_6 and C_6F_6. This suggests that the low-frequency intermolecular mode which is present in liquid C_6H_6 and C_6F_6 is absent in liquid 1,3,5-$C_6F_3H_3$. Our analysis confirms that the band can be fit by a single line shape function (eq 19), as shown in Figure 7b. The parameters for this fit are given in Table 6.

McMorrow, Lotshaw, and co-workers[15l,n] have suggested that the low-frequency component in the reduced spectral density for C_6H_6 arises from an intermolecular vibrational mode of the liquid associated with dimers or higher aggregates. They showed that this low-frequency mode is absent in a 9.1% mixture of C_6H_6 in chloroform.[15n] They attributed the disappearance of the low-frequency mode upon dilution to a shift in the dimer−monomer equilibrium in favor of the monomer. In an SGS study of liquid C_6H_6, Friedman and She[31] ascribed the low-frequency component of the vibrational band to a translational I−I mode. However, recent spectroscopic measurements of isolated benzene dimers support the interpretation of McMorrow, Lotshaw, and co-workers. In a mass-selective, ionization-detected stimulated Raman spectroscopic (IDSRS) study of jet-cooled benzene dimer isotopomers, Venturo and Felker[50] found a strong band at 10 cm^{-1} and a weaker band in the range 47−53 cm^{-1}. They have tentatively assigned these two bands to the motion of benzene moieties in two inequivalent sites. Specifically, the 10 cm^{-1} band is assigned to the hindered librational motion of the benzene moiety that forms the stem of the T, and the higher frequency band is assigned to the librational motion of the benzene moiety forming the top of the T. These bands coincide surprisingly well in frequency to the two bands found in the reduced spectral density of liquid C_6H_6. It is therefore tempting to assign the two bands in the Im[$D'(\Delta\omega)$] spectra for liquid C_6H_6 and liquid C_6F_6 to the hindered librational motions of the two benzene moieties that make up the L-shaped dimer in the liquid. In light of this interpretation, the fact that the Im[$D'(\Delta\omega)$] spectrum for liquid 1,3,5-$C_6F_3H_3$ is characterized by a single band suggests that the benzene moieties occupy equivalent sites in the dimer. This would be consistent with the parallel geometry for dimers of 1,3,5-$C_6F_3H_3$.

V. Concluding Remarks

One of the main goals of this study was to relate local order to intermolecular dynamics in aromatic liquids by doing a comparative OHD-RIKES study of benzene and nonpolar fluorinated benzene derivatives. We find indirect evidence for local order in the OHD-RIKES data for these liquids, in both the time-domain and frequency-domain representations. Using the model-dependent analysis, the intermolecular librational dynamics in C_6H_6, 1,3,5-$C_6F_3H_3$, and C_6F_6 can be characterized by oscillators with mean frequencies corresponding to $\approx$69, 31, and 33 cm^{-1}, respectively. In C_6H_6, the intermolecular librational dynamics are dominated by inhomogeneous dephasing, whereas in 1,3,5-$C_6F_3H_3$ and C_6F_6, both inhomogeneous and homogeneous dephasing processes determine the intermolecular librational dynamics. Since the librational frequencies are nearly the same for 1,3,5-$C_6F_3H_3$ and C_6F_6, the force constant governing the librational dynamics must be greater for 1,3,5-$C_6F_3H_3$ than for C_6F_6. This can be rationalized in terms of one local geometry for liquid C_6F_6 and a different local geometry for liquid 1,3,5-$C_6F_3H_3$. The reduced spectral densities obtained by using the Fourier transform approach lend further support to the local order in these liquids. For C_6H_6 and C_6F_6, the reduced spectral densities are bimodal, whereas, for 1,3,5-$C_6F_3H_3$, the reduced spectral density can ascribed to a single intermolecular vibrational mode. Previous IDSRS data for jet-cooled C_6H_6 dimers[50] suggest that the low-frequency and high-frequency intermolecular modes in the liquid are due to the librational motions of benzene moieties in inequivalent sites of a perpendicular dimer. The fact that we see a single intermolecular mode for 1,3,5-$C_6F_3H_3$ is consistent with a parallel dimer for which the sites are equivalent. To lend further credence to this interpretation of the intermolecular dynamics in these liquids, we plan to extend the OHD-RIKES study, with better signal-to-noise ratios than obtained here, to other nonpolar halogenated benzene systems and to binary mixtures of C_6F_6 and C_6H_6. The latter system is quite interesting in that C_6F_6−C_6H_6 complexes are thought to exist in these mixtures in the parallel geometry.[2,7,29]

Acknowledgment. The authors thank the reviewers of the article for their comments. This research was supported by the Texas Higher Education Coordinating Board Advanced Research Program (003644-057) and the Robert A. Welch Foundation (D-1019).

References and Notes

(1) Narten, A. H. *J. Chem. Phys.* **1968**, *48*, 1630.

(2) (a) Bartsch, E.; Bertagnolli, H.; Schulz, G.; Chiuex, P. *Ber. Bunsen-Ges. Phys. Chem.* **1985**, *89*, 147. (b) Bartsch, E.; Bertagnolli, H.; Chiuex, P. *Ber. Bunsen-Ges. Phys. Chem.* **1986**, *90*, 34.

(3) Evans, D. J.; Watts, R. O. *Mol. Phys.* **1976**, *32*, 93.

(4) Jorgensen, W. L.; Severance, D. L. *J. Am. Chem. Soc.* **1990**, *112*, 4768.

(5) Lowden, L. J.; Chandler, D. *J. Chem. Phys.* **1974**, *61*, 5228.

(6) Chandler, D. *Annu. Rev. Phys. Chem.* **1978**, *29*, 441.

(7) Vrbancich, J.; Ritchie, G. L. D. *J. Chem. Soc., Faraday Trans. 2* **1980**, *76*, 648.

(8) (a) Janda, K. C.; Hemminger, J. C.; Winn, J. S.; Novick, S. E.; Harris, S. J.; Klemperer, W. *J. Chem. Phys.* **1975**, *63*, 1419. (b) Steed, J. M.; Dixon, T. A.; Klemperer, W. *J. Chem. Phys.* **1979**, *70*, 4940.

(9) Arunan, E.; Gutowsky, H. S. *J. Chem. Phys.* **1993**, *98*, 4294.

(10) Hobza, P.; Selzle, H.; Schlag, E. W. *J. Am. Chem. Soc.* **1994**, *116*, 3500.

(11) Evans, D. A.; Chapman, K. T.; Hung, D. T.; Kawaguchi, A. T. *Angew. Chem., Int. Ed. Engl.* **1987**, *26*, 1184 and references cited therein.

(12) (a) Benzing, T.; Tjivikua, T.; Wolfe, J.; Warner, Rebek, J., Jr. *Science* **1988**, *242*, 266. (b) Muehldorf, A. V.; Van Engen, D.; Warner, J. C.; Hamilton, A. D. *J. Am. Chem. Soc.* **1988**, *110*, 6561. (c) Zimmerman, S. C.; Wu, W. *J. Am. Chem. Soc.* **1989**, *111*, 8054.

(13) Burley, S. K.; Petsko, G. A. *Science* **1985**, *229*, 23 and reference cited therein.

(14) (a) Deeg, F. W.; Stankus, J. J.; Greenfield, S. R.; Newell, V. J.; Fayer, M. D. *J. Chem. Phys.* **1989**, *90*, 6893. (b) Deeg, F. W.; Fayer, M. D. *J. Chem. Phys.* **1989**, *91*, 2269. (c) Greenfield, S. R.; Sengupta, A.; Stankus, J. J.; Terazima, M.; Fayer, M. D. *J. Phys. Chem.* **1994**, *98*, 313.

(15) (a) Kalpouzos, C.; Lotshaw, W. T.; McMorrow, D.; Kenney-Wallace, G. A. *J. Phys. Chem.* **1987**, *91*, 2028. (b) Lotshaw, W. T.; McMorrow, D.; Kalpouzos, C.; Kenney-Wallace, G. A. *Chem. Phys. Lett.* **1987**, *136*, 323. (c) McMorrow, D.; Lotshaw, W. T.; Kenney-Wallace, G. A. *J. Quantum Electron.* **1988**, *QE-24*, 443. (d) McMorrow, D.; Lotshaw, W. T.; Kenney-Wallace, G. A. In *Advances in Laser Science III, Optical Science and Engineering Series 9*; Tam, A. C. Gole, J., Stwalley, W. C., Eds.; American Institute of Physics: New York, 1988; p 674. (e) Kalpouzos, C.; McMorrow, D.; Lotshaw, W. T.; Kenney-Wallace, G. A. *Chem. Phys. Lett.* **1988**, *150*, 138. (f) Kalpouzos, C.; McMorrow, D.; Lotshaw, W. T.; Kenney-Wallace, G. A. *Chem. Phys. Lett.* **1989**, *155*, 240. (g) Lotshaw, W. T.; McMorrow, D.; Kenney-Wallace, G. A. *Proc. SPIE* **1988**, *981*, 20. (h) McMorrow, D.; Lotshaw, W. T. *Chem. Phys. Lett.* **1990**, *174*, 85. (i) McMorrow, D. *Opt. Commun.* **1991**, *86*, 236. (j) McMorrow, D.; Lotshaw, W. T. *J. Phys. Chem.* **1991**, *95*, 10395. (k) McMorrow, D.; Lotshaw, W. T. *Chem. Phys. Lett.* **1991**, *178*, 69. (l) McMorrow, D.; Lotshaw, W. T. *Chem. Phys. Lett.* **1993**, *201*, 369. (m) Palese, S.; Schilling, L.; Miller, R. J. D.; Staver, R. P.; Lotshaw, W. T. *J. Phys. Chem.* **1994**, *98*, 6308. (n) Lotshaw, W. T.; Staver, P. R.; McMorrow, D.; Thantu, N.; Melinger, J. S. *Springer Ser. Chem. Phys.* **1994**, *60*, 91. (o) Lotshaw, W. T.; McMorrow, D.; Thantu, N.; Melinger, J. S.; Kitchenham, R. *J. Raman Spectrosc.* **1995**, *26*, 571. (p) Palese, S.; Mukamel, S.; Miller, R. J. D.; Lotshaw, W. T. *J.*

Phys. Chem. **1996**, *100*, 10380. (q) McMorrow, D.; Thantu, N.; Melinger, J. S.; Kim, S. K.; Lotshaw, W. T. *J. Phys. Chem.* **1996**, *100*, 10389.

(16) (a) Chang, Y. J.; Castner, E. W., Jr. *J. Chem. Phys.* **1993**, *99*, 113. (b) Chang, Y. J.; Castner, E. W., Jr. *J. Chem. Phys.* **1993**, *99*, 7289. (c) Chang, Y. J.; Castner, E. W., Jr. *J. Phys. Chem.* **1994**, *98*, 9712. (d) Chang, Y. J.; Castner, E. W., Jr. *J. Phys. Chem.* **1996**, *100*, 3330.

(17) Cho, M.; Du, M.; Scherer, N. F.; Fleming, G. R.; Mukamel, S. *J. Chem. Phys.* **1993**, *99*, 2410.

(18) (a) Deuel, H. P.; Cong, P.; Simon, J. D. *J. Phys. Chem.* **1994**, *98*, 12600. (b) Deuel, H. P.; Cong, P.; Simon, J. D. *J. Raman Spectrosc.* **1995**, *26*, 523. (c) Cong, P.; Deuel, H. P.; Simon, J. D. *Chem. Phys. Lett.* **1995**, *240*, 72.

(19) Cong, P.; Chang, Y. J.; Simon, J. D. *J. Phys. Chem.* **1996**, *100*, 8613.

(20) (a) Ruhman, S.; Williams, L. R.; Joly, A. G.; Kohler, B.; Nelson, K. A. *J. Phys. Chem.* **1987**, *91*, 2237. (b) Ruhman, S.; Joly, A. G.; Kohler, B.; Williams, L. R.; Nelson, K. A. *Rev. Phys. Appl.* **1987**, *22*, 1717. (c) Ruhman, S.; Joly, A. G.; Nelson, K. A. *J. Quantum Electron.* **1988**, *24*, 460. (d) Kohler, B.; Nelson, K. A. *J. Phys. Chem.* **1992**, *96*, 6532.

(21) Waldman, A.; Banin, U.; Rabani, E.; Ruhman, S. *J. Phys. Chem.* **1992**, *96*, 10842.

(22) Vöhringer, P.; Scherer, N. F. *J. Phys. Chem.* **1995**, *99*, 2684.

(23) Chang, Y. J.; Cong, P.; Simon, J. D. *J. Phys. Chem.* **1995**, *99*, 7857.

(24) Keyes, T.; Ladanyi, B. M. *Mol. Phys.* **1979**, *37*, 1643.

(25) Kinoshita, S.; Kai, Y.; Yamaguchi, M.; Yagi, T. *Phys. Rev. Lett.* **1995**, *75*, 148.

(26) Gray, C. G.; Gubbins, K. E. *Theory of Molecular Fluids*; Clarendon Press: New York, 1984; Vol. 1, p 587.

(27) Riddick, J. R.; Bunger, W. B. *Organic Solvents*, Wiley-Interscience: New York, 1970.

(28) Battaglia, M. R.; Buckingham, A. D.; Williams, J. H. *Chem. Phys. Lett.* **1981**, *78*, 421.

(29) (a) Del Campo, N.; Besnard, M.; Yarwood, J. *Chem. Phys.* **1994**, *184*, 225. (b) Besnard, M.; Danten, Y.; Tassaing, T. In *Collision- and Interaction-Induced Spectroscopy*; Tabisz, G. C., Neuman, M. N., Eds.; Kluwer: Dordrecht, 1995; pp 201−213.

(30) Hattori, T.; Kobayashi, T. *J. Chem. Phys.* **1991**, *94*, 3332.

(31) (a) Friedman, J. S.; Lee, M. C.; She, C. Y. *Chem. Phys. Lett.* **1991**, *186*, 161. (b) Friedman, J. S.; She, C. Y. *J. Chem. Phys.* **1993**, *99*, 4960.

(32) Cong, P.; Simon, J. D.; She, C. Y. *J. Chem. Phys.* **1996**, *104*, 962.

(33) Neelakandan, M.; Pant, D.; Quitevis, E. L. *Chem. Phys. Lett.* **1997**, *265*, 283.

(34) Asaki, M.; Huang, C. P.; Garvey, D.; Zhou, J.; Kapteyn, H. C.; Murnane, M. M. *Opt. Lett.* **1993**, *18*, 977.

(35) Quitevis, E. L.; Neelakandan, M. *J. Phys. Chem.* **1996**, *100*, 10005.

(36) Bauer, D. R.; Brauman, J. I.; Pecora, R. *J. Chem. Phys.* **1975**, *63*, 53.

(37) Bauer, D. R.; Brauman, J. I.; Pecora, R. *J. Am. Chem. Soc.* **1974**, *96*, 6840.

(38) Dardy, H. D.; Volterra, V.; Litovitz, T. A. *J. Chem. Phys.* **1973**, *59*, 4491.

(39) Dill, J. F.; Litovitz, T. A.; Bucaro, J. A. *J. Chem. Phys.* **1975**, *62*, 3839.

(40) Yuan, P.; Chen, A. F. T.; Schwartz, M. *J. Raman Spectrosc.* **1989**, *20*, 27.

(41) Ladanyi, B. M.; Skaf, M. S.; Liang, Y. Q. In *Collision- and Interaction-Induced Spectroscopy*; Tabisz, G. C., Neuman, M. N., Eds.; Kluwer: Dordrecht, 1995; pp 143−157.

(42) Nielsen, J. R.; Liang, C.-Y.; Smith, D. C. *Trans. Faraday Soc.* **1955**, *9*, 177.

(43) Abramowitz, S.; Levin, I. W. *Spectrochim. Acta* **1970**, *26A*, 2261.

(44) Herzberg, G. *Infrared and Raman Spectroscopy*; van Nostrand-Reinhold: New York, 1945.

(45) Greene, B. I.; Fleury, P. A.; Carter, H. L., Jr.; Farrow, R. C. *Phys. Rev. A* **1984**, *29*, 271.

(46) Madden, P. A. In *Ultrafast Phenomena IV*; Auston, D. H., Eisenthal, K. B., Eds.; Springer-Verlag: New York, 1984; pp 244−251.

(47) Lynden-Bell, R. M.; Steele W. A. *J. Phys. Chem.* **1984**, *88*, 6514.

(48) As discussed in ref 15p, it is very difficult to separate the homogeneous and inhomogeneous contributions to the overall spectral density distribution of intermolecular and intramolecular degrees of freedom in a liquid from OHD-RIKES measurements. Thus, our use of homogeneous and inhomogeneous dephasing/broadening is strictly limited to the description of the librational contribution to the OKE-RIKES response in terms of the model response functions given in eqs 8 and 10.

(49) (a) Bucaro, J. A.; Litovitz, T. A. *J. Chem. Phys.* **1971**, *54*, 3846. (b) Bucaro, J. A.; Litovitz, T. A. *J. Chem. Phys.* **1971**, *55*, 3585.

(50) Venturo, V. A.; Felker, P. M. *J. Chem. Phys.* **1993**, *99*, 748.